TECHNICAL TRANSACTIONS | CZASOPISMO TECHNICZNE
FUNDAMENTAL SCIENCES | NAUKI PODSTAWOWE
1-NP/2016

WIESŁAWA BAŻELA*, MARCIN DUL*, ANDRZEJ SZYTUŁA**,
VOLODYMYR DYAKONOV***

CORRELATION BETWEEN CRYSTAL AND MAGNETIC STRUCTURE OF THE POLYCRYSTALLINE AND NANOPARTICLE $TBMNO_3$ MANGANITE

ZWIĄZEK MIĘDZY STRUKTURĄ KRYSTALICZNĄ I MAGNETYCZNĄ POLIKRYSTALICZNEJ I NANOROZMIAROWYCH PRÓBEK MANGANITU $TBMNO_3$

Abstract

On the basis of neutron diffraction data the Mn−O bond lengths and Mn−O−Mn bond angles for the poly- and nanocrystalline $TbMnO_3$ samples are determined. All the samples crystallize in the orthorhombically distorted perovskite structure (space group *Pnma*) and exhibit antiferromagnetic ordering below 41 K. The Tb atoms and O_1 atoms are in (4)c site, Mn atoms − in 4(b) site and O_2 atoms − in 8(d) site. The Mn−O_2−Mn bond angles for the polycrystalline and nanosize samples are similar, whereas the Mn−O_1−Mn bond angles for the nanoparticle samples are larger. The temperature dependencies of the Mn−O bond lengths and the Mn−O−Mn bond angles, the Jahn-Teller distortion parameter (JT) and MnO_6 − octahedron distortion parameter (delta) for polycrystalline sample exhibit anomalies at T_N temperature for Mn sublattice.

Keywords: *crystal structure, exchange interactions, nanoparticle, grain size, Mn−O bond lengths, Mn−O−Mn bond angles, the Jahn-Teller distortion parameter*

Streszczenie

Na podstawie wyników neutronowej dyfrakcji wyznaczono długości wiązań Mn–O oraz kąty wiązania Mn−O−Mn dla polikrystalicznej oraz nanorozmiarowych próbek manganitu $TbMnO_3$. Wszystkie próbki krystalizują w rombowo zdystorsowanej strukturze perowskitu (grupa przestrzenna *Pnma*) i wykazują antyferromagnetyczne uporządkowanie poniżej 41 K. Atomy Tb i tlenu O_1 zajmują pozycję 4(c), atomy Mn pozycję 4(b), a atomy tlenu O_2 pozycję 4(d). Wartości kątów wiązania Mn–O_2–Mn są zbliżone dla polikrystalicznej i nanorozmiarowych próbek związku $TbMnO_3$, podczas gdy wartości kątów wiązania Mn–O_1–Mn są wyższe dla próbek nanorozmiarowych. Temperaturowe zależności: długości wiązań Mn−O, kątów wiązania Mn–O–Mn, parametru dystorsji Jahna-Tellera (JT) oraz parametru dystorsji oktaedru MnO_6 (delta) wykazują dla próbki polikrystalicznej anomalie w temperaturze Néela dla podsieci Mn.

Słowa kluczowe: *struktura krystaliczna, oddziaływania wymiany, nanocząstki, rozmiar ziarna, długości wiązań Mn−O, kąty wiązania Mn–O−Mn, parametr dystorsji Jahna-Tellera*

DOI: 10.4467/2353737XCT.16.133.5712

* Wiesława Bażela (wbazela@pk.edu.pl), Marcin Dul, Institute of Physics, Cracow University of Technology.
** Andrzej Szytuła, M. Smoluchowski Institute of Physics, Jagiellonian University.
*** Volodymyr Dyakonov, Institute of Physics, PAS, Warsaw.

1. Introduction

The explanation of the complex magnetic interactions and correlation of the magnetic, structural and electron properties of the $REMnO_3$ (RE are the rare – earth ions) manganites is of fundamental interest [1].

$TbMnO_3$ has been attracting a lot of attention in recent years because of its strong coupling between ferroelectricity and magnetism [2].

The main motivation for performed studies was to obtain the data concerning the crystal structure and magnetic properties of the $TbMnO_3$ manganite as a function of the grain size. The model for interpretation of magnetic properties of the nanoparticle compounds is based on the ratio of ideal inner core and nonmagnetic surface, i.e., on the surface/volume ratio [3].

In this paper, we have discussed the influence of the internal structural parameters (Mn–O bond lengths and Mn–O–Mn bond angles) on the magnetic behaviour of the polycrystalline and two nanopowder $TbMnO_3$ samples. The structural distortion parameters, i.e. Jahn-Teller distortion (JT) and MnO_6 – octahedron distortion (delta) were found for all the samples.

2. Experiment and results

The polycrystalline $TbMnO_3$ manganite was prepared by the solid-state reaction. The final sintering treatment was performed at 1150ºC for 15 h. For preparation of the nanosize $TbMnO_3$ manganite the sol-gel method has been used. The two samples of the nanopowders were obtained after annealing at 800 and 850ºC [4]. The crystal structure of the samples was obtained by X-ray powder diffraction at room temperature using the Philips PW-3710 X'PERT diffractometer with CuK_α radiation. The obtained data were analysed with the Rietveld-type refinement soft-ware Fullprof program [5].

The X-ray diffraction data indicate that all the samples studied have orthorhombic crystal structure (space group *Pnma*). In this structure the Tb and O_1 atoms occupy 4(c) site: $(x, y, 1/4)$, O_2 atoms are in 8(d) site: (x, y, z) and Mn atoms are in 4(b) site: (1/2, 0, 0) (Fig.1).

The obtained data indicate that the lattice constants and positional parameters x_i, y_i, z_i slightly change with changing grain size [6]. The data for the nano-samples indicate that the *a*-constant is smaller and the *b* and *c* are larger than ones for the polycrystalline sample. All parameters have minimum at T = 30 K and quickly increase with increasing temperature.

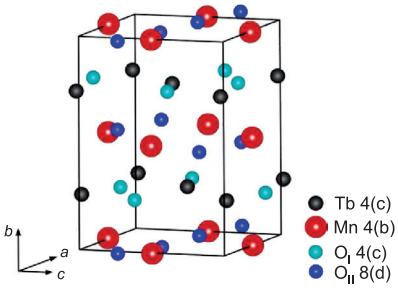

Fig. 1. The orthorhombic crystal unit cell

The grain sizes of nano-samples (800 and 850ºC) were determined using the Scherrer relation $d = \lambda/B\cos\theta_B$, where d is the grain size, λ is the X-rays wavelength, θ_B is the corresponding angle of the Bragg diffraction and B is the difference between half-widths of the Bragg reflex of the nanopowder and the standard sample [7]. The grains sizes were calculated using the experimental X-ray data and the following relation: $B = \beta - \beta_0$, where β is the half-widths of the Bragg reflex of the investigated sample and β_0 the similar value for the standard sample of Si powder with the grain size of 10 μm. The exact method of determination of grain size is described in [8]. The average grain size values determined there are: 60 nm and 45 nm for 850-nano and 800-nano samples, respectively.

In the next step, the grain sizes and strain effects were determined based on the Williamson-Hall method [9]. In this method, the broadening of Bragg peak is a sum of grain size broadening $\beta_d = K\lambda/d\cos\Theta$ and strain broadening $\beta_s = \epsilon\, tg\Theta$, where the shape factor K is close to 1, d is a value of grain size and ϵ is a strain constant.

Thus, the resulting total broadening: $\beta_{total} = \beta_s + \beta_d = \epsilon\, tg\Theta + K\lambda/d\cos\Theta$.

Multiplication of the above equation by $\cos\theta$ leads to

$$\beta_{total}\cos\Theta = \epsilon \sin\Theta + K\Theta/d.$$

Therefore, the grain size d can be determined from the intercept of line fitted with linear regression as applied to the $\beta_{total}\cos\Theta$ versus $\sin\Theta$ data.

The experimental β_{total} values have been determined from the relation:

$$\beta_{total} = [(\beta_\Theta)^2_{sample} - (\beta_\Theta)^2_{Si}]^{1/2},$$

where $(\beta_\Theta)_{sample}$ is a half – width of selected Bragg reflection of the investigated sample, while $(\beta_\Theta)_{Si}$ is a similar value found for the standard sample of Si powder.

The values of the grain size d are equal to 57 nm and 51 nm for 850-nano and 800--nano samples, respectively. Presented data indicate that the value of grain size increases with increasing annealing temperature.

The analysis presented in this paper based on the neutron diffraction powder data collected using the E2 and E6 diffractometers installed at the BERII reactor (Helmholtz--Zentrum Berlin) within the temperature range from 1.6 to 260 K. The data were processed using the program FullProf.

Neutron diffraction data [10] indicate that all the samples have orthorhombic crystal structure. Determined values of the lattice constants and atomic positions parameters are presented in Table I in [10]. Low temperature data indicate that the magnetic ordering of Mn and Tb sublattice for polycrystalline $TbMnO_3$ is sinusoidal modulated described by the propagation vector $\mathbf{k} = (k_x, 0, 0)$. The magnetic moments in Mn sublattice order below 41 K, while in Tb one they order below 9 K.

In the crystal unit cell (space group *Pnma*) the Mn^{3+} and Tb^{3+} sublattices can be described by four modes proposed by Bertaut [11]: one ferromagnetic ordering: $\mathbf{F} = m_1 + m_2 + m_3 + m_4$ and three antiferromagnetic arrangements: $\mathbf{A} = m_1 - m_2 - m_3 + m_4$, $\mathbf{C} = m_1 + m_2 - m_3 - m_4$ and $\mathbf{G} = m_1 - m_2 + m_3 - m_4$.

Below 41 K, neutron diffraction patterns for the polycrystalline sample exhibit additional magnetic peaks connected with the antiferromagnetic modulated ordering with $k_x = 0.28$ in Mn sublattice described by $\mathbf{C_x}$ – mode (see Fig. 1a in [6]).

The Mn magnetic moments, parallel to the *a*-axis, form a collinear incommensurate structure of $\mathbf{C}_x$ – mode. At T = 16 K a noncollinear magnetic structure described by $\mathbf{C}_x\mathbf{A}_z$ – mode with the Mn moment in the *a*–*c* plane was observed (see Fig. 2).

The Tb sublattice exhibits the antiferromagnetic incommensurate ordering of the $\mathbf{F}_y\mathbf{A}_z$ – type at T = 5 K. The Tb magnetic structure is described by propagation vector $\mathbf{k} = (k_x, 0, 0)$ where k_x is equal to 0.423(1) (Fig. 2). At the same temperature, the Mn moments still form the $\mathbf{C}_x\mathbf{A}_z$ structure described by propagation vector $\mathbf{k} = (k_x, 0, 0)$ where k_x is equal to 0.282(1).

The refinement of the magnetic peaks intensities for the nano-800 and nano-850 samples below T_N shows that the Mn moments form a collinear incommensurate magnetic structure of $\mathbf{C}_x$ – type described by the propagation vector $\mathbf{k} = (k_x, 0, 0)$ (see Fig. 3). The corresponding patterns for the nano-800 and nano-850 samples are presented in Figs. 1b and 1c in [6]. At 1.6 K, the additional peaks connected to the Tb moments ordering are visible. The Tb structure can be described by the $\mathbf{A}_z$ – mode with propagation vector $\mathbf{k} = (k_x, 0, 0)$ (see Fig. 3), while for the polycrystalline sample the $\mathbf{F}_y\mathbf{A}_z$ – mode was evidenced.

The Mn magnetic moments values for nano-samples (at 1.6 K μ(Mn) = 2.94(2) μ_B and 3.03(4) μ_B for nano-800 and nano-850, respectively) are smaller than for the polycrystalline sample (at 5 K μ(Mn) = 4.06(2) μ_B), whereas for the nano-samples the k_x components equal to 0.321(2) and 0.328(2) for nano-800 and nano-850, respectively, are larger than in the polycrystalline sample (0.282(1)).

Similar conclusions concern the parameters characterizing the ordering in Tb sublattice. At 1.6 K μ(Tb) = 3.68(11) μ_B and 4.43(7) μ_B for nano-800 and nano-850, respectively.

For polycrystalline sample μ(Tb) is equal to 6.55(4) μ_B at 5 K. The values of k_x component for Tb sublattice are larger for nano-samples (0.443(5) and 0.451(3) for nano-800 and nano--850, respectively.

The T_N Néel temperature connected with the Tb sublattice is lower for nano-samples (6.7 K) in comparison to polycrystalline sample (9 K).

Magnetic structures of the polycrystalline and nanoparticle $TbMnO_3$ compounds are presented in Figs. 2 and 3, respectively. These magnetic structures are incommensurate

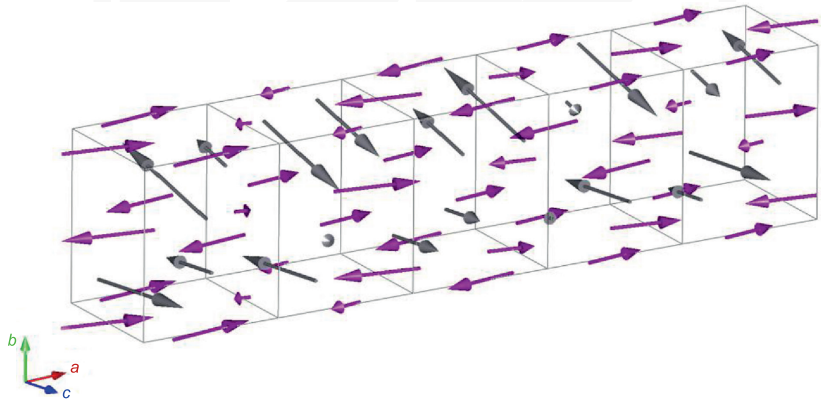

Fig. 2. Sinusoidal magnetic ordering in Mn sublattice – violet ($\mathbf{C}_x\mathbf{A}_z$ – mode, k_x = 0.282(1)) and in Tb sublattice – black ($\mathbf{F}_y\mathbf{A}_z$ – mode, k_x = 0.423(1)) for polycrystalline $TbMnO_3$

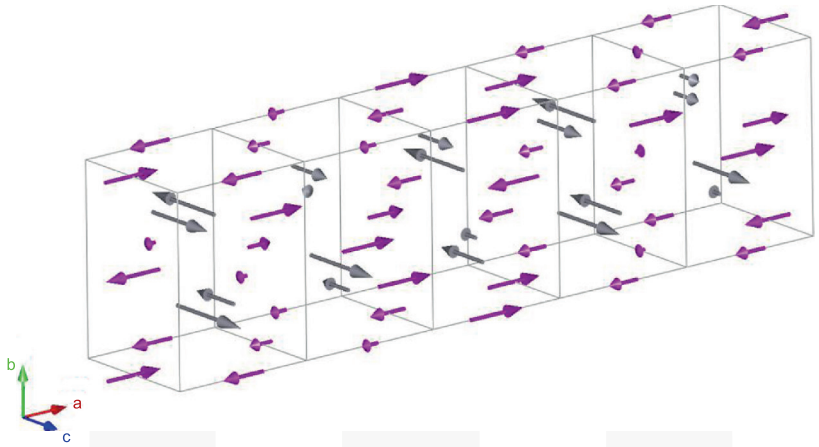

Fig. 3. Sinusoidal magnetic ordering in Mn sublattice – violet ($\mathbf{C}_x$ – mode, $k_x = 0.326(4)$) and in Tb sublattice – black ($\mathbf{A}_z$ – mode, $k_x = 0.443(5)$) for 800-nano $TbMnO_3$

in comparison with the crystal one. The periods of modulation of the magnetic structure are equal to 3.54*a* (Mn sublattice) and 2.36*a* (Tb sublattice) for polycrystalline sample and 3.06*a* (Mn) and 2.25*a* (Tb) for nano-samples, respectively.

In this paper we have focused on the behaviour of the internal structural parameters in the polycrystalline and two nanoparticle samples (Mn–O bond lengths and Mn–O–Mn bond angles) as a function of temperature. In the orthorhombic unit cell there are the three crystallographically independent ($Mn–O_I(4c) = r_1$, $Mn–O_2(8d)_1 = r_2$, $Mn–O_2(8d)_2 = r_3$) bond lengths and the two ($Mn–O_1–Mn = \alpha$, $Mn–O_2–Mn = \beta$) bond angles (Fig. 4). The temperature dependencies of the Mn–O bond lengths and Mn–O–Mn bond angles for the polycrystalline and two nanoparticle $TbMnO_3$ samples are presented in Fig. 5.

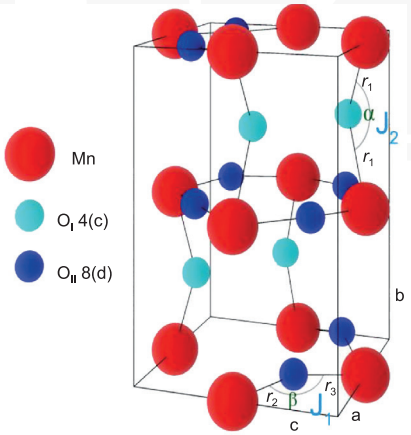

Fig. 4. The orthorhombic crystal unit cell with the marked Mn–O bond lengths (r_1, r_2, r_3) and Mn–O–Mn bond angles (α, β) and the exchange integrals J_1, J_2

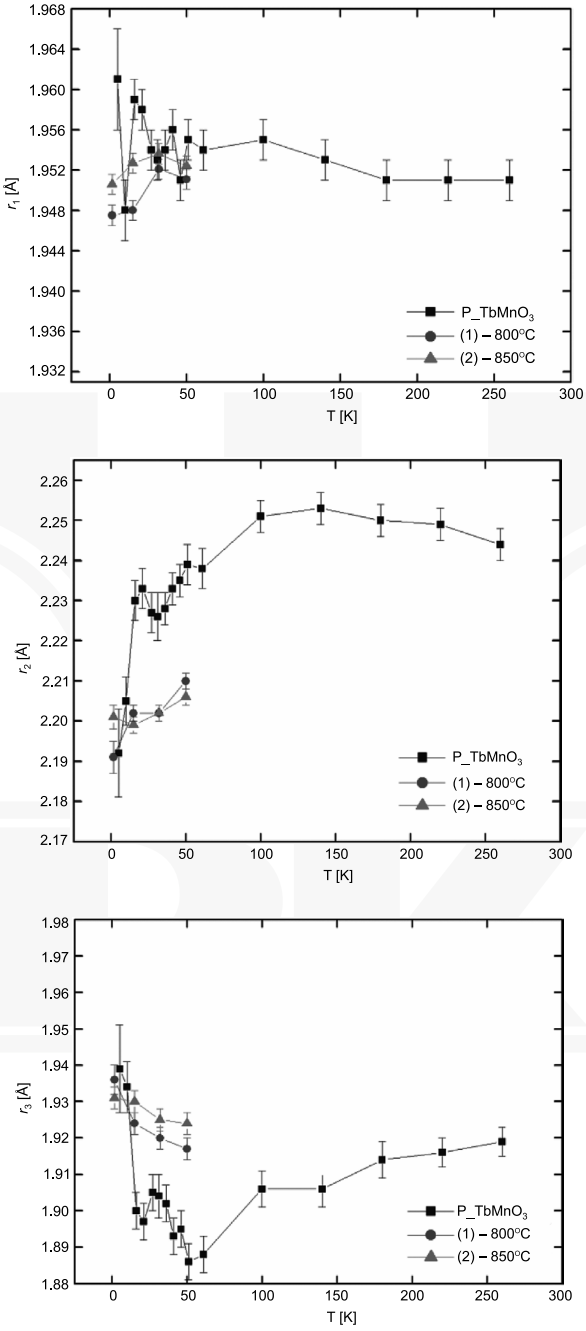

Fig. 5. Mn–O bond lengths (r_1, r_2, r_3) as a function of temperature for polycrystalline and 800 and 850-nano-samples of $TbMnO_3$

The temperature dependencies of the r_1 and r_2 bond lengths show that r_1 and r_2 are smaller for the nanosize samples as compared to the polycrystalline sample (see Fig. 5). This suggests that in these samples there are a greater overlap of *p* and *d* orbitals.

We have observed an increase of the r_1 and r_2 bond lengths for the nanosize samples with approaching to the Néel temperature. For the polycrystalline sample above T = 50 K the stabilization of all three r_1, r_2 and r_3 bond lengths is visible. The dependence of r_3(T) exhibits an inverse behaviour as compared to r_2(T) (see Fig. 5).

Fig. 6 presents a gradual increase of the α bond angle vs temperature for the polycrystalline sample, whereas for the nanosize samples a decrease of α till to the Néel temperature and an increase beyond T_N is observed. The α bond angles are larger for the nanoparticle samples as compared to α for the polycrystalline sample.

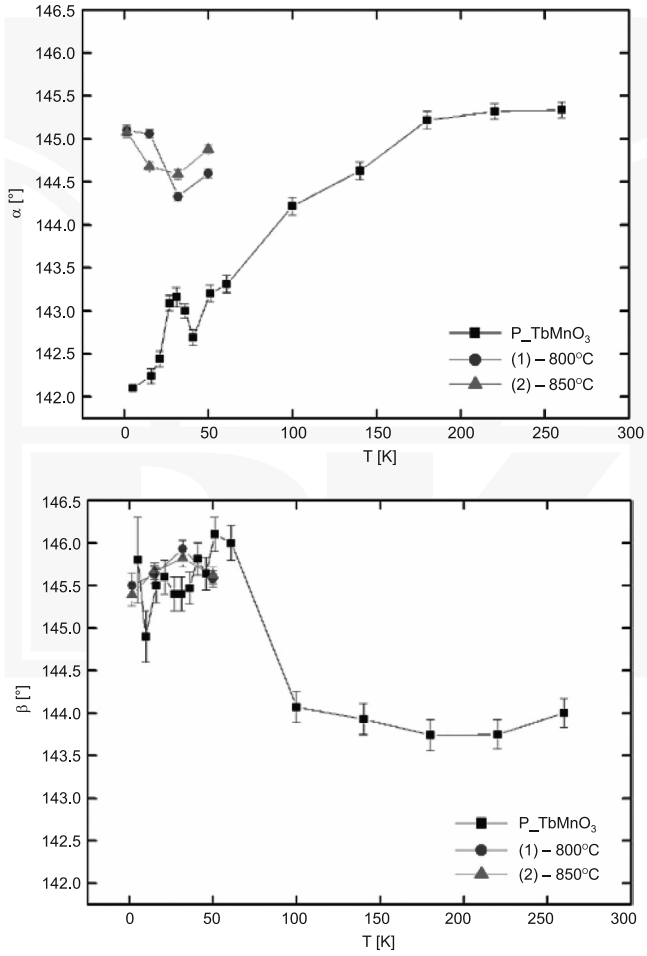

Fig. 6. Mn–O–Mn bond angles (α, β) as a function of temperature for the polycrystalline and 800-nano and 850-nano $TbMnO_3$ samples

This suggests an increase of superexchange interactions along the *b*-axis. Values of β bond angle are similar for the nano- and poly-$TbMnO_3$ samples. For both types of samples an increase of β is observed till the Néel temperature. Beyond this temperature the β bond angle value substantially drops. Using the r_1, r_2 and r_3 bond lengths the Jahn-Teller parameter [12] for the polycrystalline and nanosize samples has been determined according to the formula [13]:

$$JT = \sqrt{\frac{1}{3}\sum_{i=1}^{3}[(r_i) - < r >]^2}$$

where r_i are the experimentally determined values of (Mn–O) interatomic lengths (see Fig. 4) and $< r >$ is the average value of these lengths.

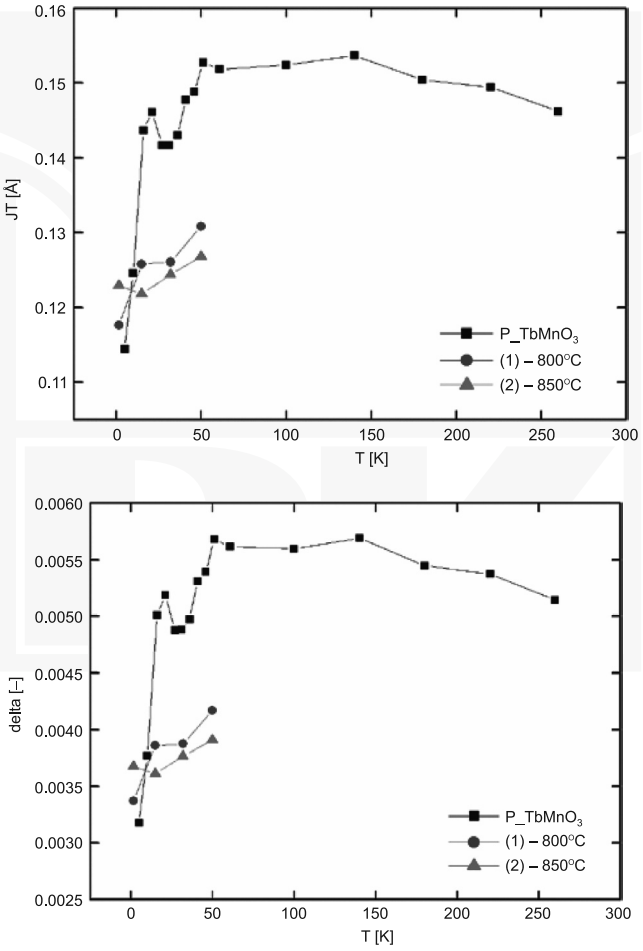

Fig. 7. Temperature dependences of the Jahn-Teller parameter (JT) and the parameter delta for the polycrystalline and nanosize samples of $TbMnO_3$

The parameter delta, which describes the distortion of MnO_6 octahedron is calculated using the formula:

$$\text{delta} = \frac{1}{3}\sum_{i=1}^{3}\left[\frac{r_i - < r >}{< r >}\right]^2$$

Temperature dependences of the Jahn-Teller parameter (JT) and the parameter delta for the polycrystalline and nanosize samples of $TbMnO_3$ are presented in Fig. 7.

The values of both the Jahn-Teller parameter and the delta parameter indicate the MnO_6 octahedron distortion. Distortion is much smaller for the nanocrystalline samples than for polycrystalline one. For polycrystalline sample the Jahn-Teller parameter has anomaly at Néel temperature.

3. Discussion

The data presented in this paper indicate that the magnetic properties of the nanoparticle samples strongly depend on the grain size. This manifests itself in decrease of the value of both magnetic moments in the ordered state and magnetic ordering temperature with decreasing grain size.

The $TbMnO_3$ manganite exhibits a para- antiferromagnetic phase transition at 41 K, where the Mn^{3+} ions develop a sinusoidal incommensurate ordering propagating along the *a* – direction of the unit cell, described by $\mathbf{C_xA_z}$ – mode. Magnetic order in the Mn sublattice is collinear of $\mathbf{C_x}$ – type in the temperature range of 21–41 K. For the investigated nano--samples a magnetic ordering in the Mn sublattice is described by collinear $\mathbf{C_x}$ – mode only.

Observed antiferromagnetic order in the Mn sublattice is result of the superexchange mechanism (cation-anion-cation) which exists in manganites. The superexchange interaction depends on the Mn–O–Mn bond angles (α, β) and is joined with partial overlap of the *p* (O) and *d* (Mn) orbitals. The interactions between Mn moments are based on the exchange integrals discussed by Bertaut [14].

At temperature 1.6 K, the values of α and β bond angles are equal to 142º and 146º for the polycrystalline sample while they are equal to 145º and 145.5º for the nanoparticle samples, respectively.

The obtained values of the Mn–O–Mn bond angles (α, β) are smaller than 180º. This fact indicates the moderate ferro- or antiferromagnetic interaction between magnetic moments of Mn according to the Goodenough-Kanamori rules [15, 16].

Analysis of interactions in the orthorhombic manganites with magnetic structure described by the propagation vector $\mathbf{k} = (k_x, 0, 0)$ gives the following dependence between k_x and exchange integrals: $\cos(\pi k_x) \approx (2J_2 - J_1)$ [17], where J_1 is the exchange integral in the basal *a*–*c* plane [t_{2g}(Mn) – $2p_\pi$ (O) – t_{2g} (Mn)] and J_2 is the exchange integral along the *b*-axis [e_g(Mn) – $2p_\pi$ (O) – e_g (Mn)].

The inelastic neutron scattering for the bulk $TbMnO_3$ yields the positive value of $J_1 \approx 0.15(1)$ meV and negative one of $J_2 \approx -0.31(2)$ meV [18]. This result confirms, that for the $TbMnO_3$ manganite the superexchange interaction between Mn–O_2–Mn spins in the *a*–*c* plane (J_1) is ferromagnetic, while the interaction Mn–O_1–Mn along the *b*-axis

is antiferromagnetic (J_2) (see Fig. 4). An increase of the k_x component observed in the nanoparticle $TbMnO_3$ sample indicates the decrease of the exchange integrals in nano--samples.

The presented results suggest that the nanoparticle size plays an important role in the formation of magnetic properties. The influence of deformation of the MnO_6-octahedron on the magnetic structure of $TbMnO_3$ manganite is observed. The values of Mn–O_2–Mn bond angles in the polycrystalline and nanosize samples are similar and the temperature dependences exhibit anomalies at T_N temperature. The values of the Mn–O_1–Mn bond angles are larger for the nanoparticle samples.

For nano-samples the Jahn-Teller distortion parameter (JT) and MnO_6-octahedron distortion parameter (delta) are lowered in comparison to the polycrystalline sample.

References

[1] Dagotto E., *Nanoscale Phase Separation and Colossal Magnetoresistance*, Springer-Verlag, Berlin 2001.

[2] Kimura T., Goto T., Shintani H., Ishizaka K., Arima T., Tokura Y., *Magnetic control of ferroelectric polarizatoin*, Nature 426, 2003, 55-58.

[3] Lopez-Quintela M.A., Huesco L.E., Rivas J., Rivandulla F., *Intergranular magnetoresistance in nanomanganites*, "Nanotechnology" 14, 2003, 212-219.

[4] Dyakonov V., Szytuła A., Szymczak R., Zubov E., Szewczyk A., Kravchenko Z., Bażela W., Dyakonov K., Zarzycki A., Varyukhin V., Szymczak H., *Phase transitions in $TbMnO_3$*, Low Temperature Physics, 38, 1, 2012.

[5] Rodriguez-Carvajal J., *Recent advances in magnetic structure determination by neutron powder diffraction*, Physica B 192, 1993, 55-69.

[6] Bażela W., Dul M., Dyakonov V., Gondek Ł., Hoser A., Hoffmann J.-U., Penc B., Szytuła A., Kravchenko Z., Nosalev I., Zarzycki A., *Infuence of the grain size on the magnetic properties of $TbMnO_3$*, Acta Physica Polonica A, Vol. 121, No. 4, 2012, 785-788.

[7] Rasberry S.D., *Bureau of Standards Certicate-Standard Reference Material 640b*, 1987.

[8] Dul M., Bażela W., *The determination of crystal structure and grain size of $La_{0.7}Sr_{0.3}MnO_3$*, Czasopismo Techniczne (Technical Transations) 1-NP/2010, Issue 1, Year 107, 2010, p. 71-91.

[9] Williamson G.K., Hall W.H., *X-ray line broadening from filled aluminium and wolfram*, Acta Metallurgica 1, 1953, 22-31.

[10] Bażela W., Dul M., Dyakonov V., Gondek Ł., Hoser A., Hoffmann J.-U., Penc B., Szytuła A., Kravchenko Z., Nosalev I., Zarzycki A., *Magnetic and neutron diffraction studies of the polycrystalline and nanoparticle $TbMnO_3$*, Acta Physica Polonica A 122, 2012, 384-390.

[11] Bertaut E. F., *Spin configuration of ionic structures: theory and practice in: Magnetism*, Vol III, Eds. Rado G.T., Shul H., Academic Press, N.Y. 1963, p.149-209.

[12] Radaelli P.G., Iaonne G., Marezio M., Hwang H.Y., Cheong S.-W., Jorgensen J.D., Argyrion D.V., *Structural effects on the magnetic and transport properties of perovskite $A_{1-x}A'_xMnO_3$*, Physical Review B, 56, 1997, 8265-8276.

[13] Radaelli P.G., Marezio M., Hwang H.Y., Cheong S.-W., Batlogg B., *Charge localization by static and dynamic distortions of the MnO_6 octahedra in perovskite manganites*, Physical Review B, 54, 1996, 8992-8995.

[14] Bertaut E.F., *Representation analysis of magnetic structures*, Acta Crystallographica A24, 217, 1963.

[15] Goodenough J.B., *An interpretation of the magnetic properties of the perovskite – type mixed crystal* $La_{1-x}Sr_xCoO_{3-x}$, Journal of Physics and Chemistry of Solids, 6, 1958, 287-297.
[16] Kanamori J., *Superexchange interaction and symmetry properties of electron orbitals*, Journal of Physics and Chemistry of Solids, 10, 1959, 87-98.
[17] Brinks H.W., Rodrigues-Carvajal J., Fjellvag H., Kjaksus A., Hauback B.C., *Crystal and magnetic structure of orthorhombic* $HoMnO_3$, Physical Review B 63, 094411-094412, 2001.
[18] Senff D., Link P., Hradil K., Hiess A., Regnault L.P., Sidis Y., Aliouane N., Argyrion D.V., Braden M., *Magnetic excitations in multiferroic* $TbMnO_3$*: evidence for a hybridized soft mode*, Physical Review Letters, 98, 137206, 2007.